UC Irvine
UC Irvine Electronic Theses and Dissertations

Title

Exploring Higher Accuracy Poisson-Boltzmann Methods for Biomolecular Simulations

Permalink

Author

Wang, Changhao

Publication Date

2016

Peer reviewed|Thesis/dissertation

UNIVERSITY OF CALIFORNIA
IRVINE

Exploring Higher Accuracy
Poisson-Boltzmann Methods for Biomolecular Simulations

THESIS

submitted in partial satisfaction of the requirements
for the degree of

MASTER OF SCIENCE

in Chemical and Materials Physics

by

Changhao Wang

Thesis Committee:
Professor Ray Luo, Chair
Professor Ioan Andricioaei
Professor Ruqian Wu

2016

TABLE OF CONTENTS

Page

LIST OF FIGURES

Page

LIST OF TABLE

ACKNOWLEDGMENTS

ABSTRACT OF THE THESIS

Exploring Higher Accuracy
Poisson-Boltzmann Methods for Biomolecular Simulations

By

Changhao Wang

Master of Science in Chemical and Materials Physics – Physics

University of California, Irvine, 2016

Professor Ray Luo, Chair

Accurate and efficient treatment of electrostatics is a crucial step in computational analyses of biomolecular structures and dynamics. In this study, we have explored a second-order finite-difference numerical method to solve the widely used Poisson-Boltzmann equation for electrostatic analyses of realistic biomolecules. The so-called immersed interface method was first validated and found to be consistent with the classical weighted harmonic averaging method for a diversified set of test biomolecules. The numerical accuracy and convergence behaviors of the new method were next analyzed in its computation of numerical reaction field grid potentials, energies, and atomic solvation forces. Overall similar convergence behaviors were observed as those by the classical method. Interestingly, the new method was found to deliver more accurate and better-converged grid potentials than the classical method on or nearby the molecular surface, though the numerical advantage of the new method is reduced when grid potentials are

extrapolated to the molecular surface. Our exploratory study indicates the need for further improving interpolation/extrapolation schemes in addition to the developments of higher-order numerical methods that have attracted most attention in the field.

CHAPTER 1: Introduction

Electrostatic interactions play important roles in the structural, dynamic and functional properties of biomolecules. Accurate and efficient treatment of electrostatics is thus crucial in computational analyses of biomolecular structures and dynamics. A closely related issue is the modeling of water molecules and their electrostatic interactions with biomolecules that must be considered for any realistic representation of biomolecules at physiological conditions. Since most particles in a molecular model represent water molecules solvating the target biomolecules, treating these water molecules implicitly offers an opportunity to reach higher computational efficiency to model more complex biomolecular systems. A class of successful implicit solvent models based on the Poisson-Boltzmann equation (PBE) has been widely accepted for biomolecular applications after years of basic research and development.

In this implicit/continuum solvent treatment, the solute molecule is treated as a low dielectric constant region and the solvent is treated as a high dielectric constant region. A number of fixed interior point charges are located atomic centers. Since analytic solution of the PBE can be achieved only in a few specific cases with simple solute geometry, a numerical solution of the PBE is needed for biomolecular applications. Among the numerical solution methods, finite-difference methods (FDM) [1-14], finite-element methods (FEM) [15-24] and boundary-element methods (BEM) [25-42] are mostly used. In these three methods, FDM has the advantage of the straightforward and physically transparent nature of the calculation. However, if a direct discretization is used without considering the discontinuity in the dielectric

constant, the numerical solutions tend to have large errors, and the errors are particularly obvious near the solute-solvent interface. To overcome this problem, Davis and McCammon proposed a harmonic average (HA) method to approach the approximate dielectric constant near surface in 1991 [43]. Efforts have also been reported recently by Wei and co-workers and Li and co-workers to develop higher accuracy interface schemes, the matched interface and boundary (MIB) method and immersed interface method (IIM), to improve numerical accuracy of the PBE solution [44-48]. The scheme of MIB is enforcing the lowest-order jump condition repeatedly to achieve the high-order jump condition. On the other hand, the idea of IIM is to enforce the interface conditions into the finite-difference schemes at grid points near the interface. Besides these higher-order numerical schemes, there are also proposals to improve implicit solvent model, including coupling electrostatic and nonelectrostatic interactions within the implicit solvation treatment [49-53] and using level set to help the definition of solvent-solute interface [54, 55].

Even with constant community-wide efforts to improve the efficiency and accuracy of numerical PBE models, mathematical and computational challenges remain in adoption of the methods to routine molecular dynamics simulations. One challenge is the difficulty of assigning forces related to the dielectric boundary to individual atoms, and many efforts have been invested to develop methods to compute electrostatic forces [7, 15, 21, 30, 56-73]. Another challenge is how to achieve convergence of numerical energy and forces with respect to the resolution of the solute-solvent boundary and charge representation efficiently both in terms of CPU time and memory usage [43, 74]. Indeed, numerical forces are especially difficult to reach a

high enough accuracy because forces are derivatives of energies that are always harder than energies to compute by numerical approaches. These issues still limit the applications of numerical PBE models to calculations involving static biomolecular structures only.

In this study, we explored a higher-accuracy numerical scheme, the immersed interface method (IIM), to solve the PBE [75]. The idea of IIM is to enforce the interface conditions into the finite-difference schemes at grid points near the interface. Our preliminary analysis on the IIM for a well-studied analytical system indicated its promises for biomolecular applications [76]. Here we extended the IIM to realistic biomolecules to investigate its performance of electrostatic properties, such as gird reaction field potential, atomic reaction field energy and atomic reaction field forces. In addition, interface properties such as potentials and electric fields were also carefully analyzed for future applications in dielectric stress and pressure calculations.

CHAPTER 2: Theory

2.1 Finite-difference/finite-volume method

Without loss of generality, we focus on the Poisson's equation in this study since the Boltzmann term is nonzero only outside the Stern layer, which is typically set 2 Å away from the dielectric interface where the dielectric constant is smooth. The partial differential equation

$$\nabla \cdot \varepsilon \nabla \phi = -4\pi\rho \tag{1}$$

establishes a relation between charge density (ρ) and electrostatic potential (ϕ), given a predefined dielectric distribution function (ε) for a solvated molecule.

The FDM is a widely utilized numerical method to discretize partial differential equations. With FDM, a uniform Cartesian grid is used to discretize a finite rectangle box containing the solvated molecule. The grid points are numbered as (i, j, k), $i = 1,...,xm, j = 1,...,ym, k = 1,...,zm$, where xm, ym and zm are the numbers of points along the x, y, and z axes, respectively. The spacing between neighbor points is uniformly set to be h. Charge density $\rho(i,j,k)$ in FDM is given as $\rho(i,j,k) = q(i,j,k)/h^3$, where the $q(i,j,k)$ is the total charge within the cubic volume centered at (i, j, k). Under this discretization scheme, the Poisson's equation can be discretized as

$$\{\varepsilon(i-\frac{1}{2},j,k)[\phi(i-1,j,k)-\phi(i,j,k)]$$

$$+\varepsilon(i+\frac{1}{2},j,k)[\phi(i+1,j,k)-\phi(i,j,k)]$$

$$+\varepsilon(i,j-\frac{1}{2},k)[\phi(i,j-1,k)-\phi(i,j,k)]$$

$$+\varepsilon(i,j+\frac{1}{2},k)[\phi(i,j+1,k)-\phi(i,j,k)] \quad\quad (2)$$

$$+\varepsilon(i,j,k-\frac{1}{2})[\phi(i,j,k-1)-\phi(i,j,k)]$$

$$+\varepsilon(i,j,k+\frac{1}{2})[\phi(i,j,k+1)-\phi(i,j,k)]\}/h^2 =$$

$$-4\pi q(i,j,k)/h^3,$$

where h is the spacing in each dimension; $\phi(i,j,k)$ is the potential on grid (i, j, k), and

$\phi(i\pm1,j,k)$, $\phi(i,j\pm1,k)$ and $\phi(i,j,k\pm1)$ are defined similarly; $\varepsilon(i-\frac{1}{2},j,k)$ is the dielectric

constant at the mid-point between grids (i, j, k) and $(i\text{-}1, j, k)$, and $\varepsilon(i,j-\frac{1}{2},k)$ and

$\varepsilon(i,j,k-\frac{1}{2})$ are defined similarly; $\varepsilon(i+\frac{1}{2},j,k)$ is the dielectric constant at the mid-point

between grids (i, j, k) and $(i\text{+}1, j, k)$, and $\varepsilon(i,j+\frac{1}{2},k)$ and $\varepsilon(i,j,k+\frac{1}{2})$ are defined similarly.

The dielectric constant is related to the dielectric interface treatment to be discussed below. The

solute atomic charge distribution is mapped onto grid points using a mapping procedure. Here

the trilinear mapping method was used [77]. More detailed implementation information can be

found in our recent works [9, 11, 13, 14, 78].

2.2 Interface treatment: Harmonic average

Harmonic average is a well-established interface treatment method. For FDM, the dielectric

constant is difficult to set when the two neighboring grid points belong to different dielectric regions. The electrostatic interface/jump condition must be satisfied across the interface between the different dielectric regions. One simple treatment is the use of harmonic average (HA) of the two dielectric constants at the interface midpoints to satisfy the jump condition in each dimension [43]. For example, if $(i-1, j, k)$ and (i, j, k) belong to different dielectric regions, there must be an interface point on the grid edge between $(i-1, j, k)$ and (i, j, k). In HA, $\varepsilon(i-\frac{1}{2}, j, k)$ is defined as

$$\varepsilon(i-\frac{1}{2}, j, k) = \frac{h}{\frac{a}{\varepsilon(i-1, j, k)} + \frac{b}{\varepsilon(i, j, k)}}, \tag{3}$$

where a is the distance from the interface point to grid point $(i-1, j, k)$, and b is the distance from the same interface point to grid point (i, j, k). Obviously, this is an approximated treatment, but this strategy has been shown to improve the convergence of reaction field energies respect to the grid spacing [43].

2.3 Interface treatment: Immersed interface method

A more systematic way for interface treatment is the immersed interface method (IIM) [75]. In IIM the interface is often represented by the zero level set of a Lipchitz continuous function (often the signed distance function) $\varphi(x, y, z)$:

$$\begin{aligned} \varphi(x, y, z) &< 0 \quad if \ (x, y, z) \in \Omega^- \\ \varphi(x, y, z) &= 0 \quad if \ (x, y, z) \in \Gamma \\ \varphi(x, y, z) &> 0 \quad if \ (x, y, z) \in \Omega^+, \end{aligned} \tag{4}$$

where Γ is the interface, Ω^- is the inside dielectric region and Ω^+ is the outside dielectric regions. After defining

$$
\begin{aligned}
\varphi_{ijk}^{min} &= \min\{\varphi(i\pm1,j,k),\varphi(i,j\pm1,k),\varphi(i,j,k\pm1)\} \\
\varphi_{ijk}^{max} &= \max\{\varphi(i\pm1,j,k),\varphi(i,j\pm1,k),\varphi(i,j,k\pm1)\},
\end{aligned}
\tag{5}
$$

a grid point can be classified irregular if $\varphi_{ijk}^{min}\varphi_{ijk}^{max}\leq0$, and regular if otherwise.

Discretized partial differential equation is given as same as Eqn (2):

$$
\begin{aligned}
\{&\varepsilon(i-\tfrac{1}{2},j,k)[\phi(i-1,j,k)-\phi(i,j,k)] \\
+&\varepsilon(i+\tfrac{1}{2},j,k)[\phi(i+1,j,k)-\phi(i,j,k)] \\
+&\varepsilon(i,j-\tfrac{1}{2},k)[\phi(i,j-1,k)-\phi(i,j,k)] \\
+&\varepsilon(i,j+\tfrac{1}{2},k)[\phi(i,j+1,k)-\phi(i,j,k)] \\
+&\varepsilon(i,j,k-\tfrac{1}{2})[\phi(i,j,k-1)-\phi(i,j,k)] \\
+&\varepsilon(i,j,k+\tfrac{1}{2})[\phi(i,j,k+1)-\phi(i,j,k)]\}/h^2 \\
=&f(i,j,k)=-4\pi q(i,j,k)/h^3,
\end{aligned}
\tag{6}
$$

where $f(i,j,k)$ is used to denote the point charge term, and two interface conditions on interface Γ as

$$
\begin{aligned}
[\phi]_\Gamma &= w \\
[\varepsilon\phi_n]_\Gamma &= v.
\end{aligned}
\tag{7}
$$

Here, $[u]_\alpha$ is defined as $[u]_\alpha=u(\alpha^+)-u(\alpha^-)=\lim\limits_{x\to\alpha^+}u(x)-\lim\limits_{x\to\alpha^-}u(x)$. A new set of finite-difference equations involves 27 points including one irregular point and 26 neighboring points of the irregular point in a 3×3×3 grid cube. These new equations consist of the matrix of IIM instead of the original 7-point finite-difference equations at irregular points.

The new finite difference equation at irregular point (i, j, k) can be written as

$$\sum_{m}^{n_s} \gamma_m \phi(i+i_m, j+j_m, k+k_m) = f(i,j,k) + C(i,j,k), \qquad (8)$$

where n_s represents all the 27 grid points, γ_m are the undetermined coefficients, and $C(i,j,k)$ is an undetermined correction term, chosen to minimize the local truncation error while satisfying the interface conditions of $[\phi]_\Gamma = w$ and $[\varepsilon\phi_n]_\Gamma = v$. The basic idea of IIM is to determine γ_m in Eqn (8) at the irregular points so that the second-order global accuracy is obtained as in an interface-free problem with the finite-difference/finite-volume discretization scheme. Since only grid points nearby the interface are involved, it is sufficient to have an $O(h)$ local truncation error at those points to reach the goal [75, 79]. The detailed procedure has been documented in our previous works [76].

2.4 Removal of charge singularity

Point charge models are widely used in molecular dynamics of biomolecules, yet the representation of point charges is delta function that is difficult to solve by PB equations. Eqn (2) shows that the finite-volume discretization scheme overcomes this problem by resorting to the integral form of the PBE. Thus the total charge, instead of the singular charge density, appears as a discretized form $q(i,j,k)$ in the right side of Eqn (2) at grid point (i,j,k). However, such a treatment will introduce the singularity at the gird points to distort the Coulombic potential especially when it is close to a grid charge [65].

Several advanced strategies are also available to remove the charge singularity [19, 45, 80,

8

81]. Here we adopted an efficient strategy developed by our group [82]. We explain this approach briefly. The reaction field potential (ϕ_{RF}) is solved in the solute region (Ω^-) and the total potential ($\phi = \phi_{RF} + \phi_C$) is solved in the solvent region (Ω^+). Here ϕ_C is the Coulombic potential, satisfying $\varepsilon_- \nabla^2 \phi_C = -4\pi\rho$ [82]. The respective equations for ϕ_{RF} and ϕ are

$$\begin{cases} \nabla \cdot \varepsilon \nabla \phi_{RF} = 0, & in\ \Omega^- \\ \nabla \cdot \varepsilon \nabla \phi - N(\phi) = 0, & in\ \Omega^+ \end{cases}, \tag{9}$$

where $N(\phi)$ represents the Boltzmann term and is set to zero in the current study [82]. The corresponding interface conditions across Γ are then

$$\begin{cases} \phi = \phi_C + \phi_{RF} \\ \left[\varepsilon \dfrac{\partial \phi_{RF}}{\partial n} \right] = -\left[\varepsilon \dfrac{\partial \phi_C}{\partial n} \right]. \end{cases} \tag{10}$$

As shown in Eqn (10), the Coulombic potential is needed on the interface [82].

2.5 Electrostatic energy and forces

2.5.1 Reaction field energy and forces

The reaction field energy (ΔG) is calculated as

$$\Delta G = \frac{1}{2} \sum_{i=1}^{N_q} q_i (\phi - \phi_C). \tag{11}$$

If the charge singularity is removed, it is simply

$$\Delta G = \frac{1}{2} \sum_{i=1}^{N_q} q_i \phi_{RF}. \tag{12}$$

The reaction field forces (qE) are obtained as

9

$$\mathbf{F}_{qE} = \sum_{i=1}^{N_q} q_i \mathbf{E}_{RF}. \tag{13}$$

2.5.2 Interface potential and electrostatic field

After solving the finite-difference equations, only potential values at grid points are known. To obtain potential or electrostatic field at any position (x_0, y_0, z_0), we utilized the one-sided least-square fitting method [79]. Briefly, there are $N(\geq 10)$ equations of the second-order 3D-Taylor expansion, respectively, for the $N(\geq 10)$ grid points with respect to the origin, (x_0, y_0, z_0), i.e. the surface point of interest

$$\begin{aligned} f(x,y,z)_i = & A_1 + A_2(x-x_0)_i + A_3(y-y_0)_i + A_4(z-z_0)_i \\ & + A_5(x-x_0)_i^2 + A_6(y-y_0)_i^2 + A_7(z-z_0)_i^2 \\ & + A_8(x-x_0)_i(y-y_0)_i + A_9(y-y_0)_i(z-z_0)_i \\ & + A_{10}(x-x_0)_i(z-z_0)_i \end{aligned} \tag{14}$$

These equations are involved to determine the coefficients A_α, $\alpha = 1, ..., 10$, where $f(x,y,z)_i$ is the potential of grid point $(x,y,z)_i$, and $(x-x_0)_i$, $(y-y_0)_i$ and $(z-z_0)_i$ are the relative position vector components of grid point $(x,y,z)_i$ with respect to the origin (x_0, y_0, z_0). The $N(\geq 10)$ grid points are chosen to be within a 3×3×3 cubic grid, where the center point is the nearest grid point to the origin. Since we are to conduct a one-side extrapolation, only the inside grid points are included. Within the cubic grid, about half of the 27 points are each side of the interface so that the number of grid points $N(\geq 10)$ selected in the fitting is in the range of 10 ~ 18. The coefficients A_α, $\alpha = 1, ..., 10$ are then solved by the Singular Value Decomposition (SVD) algorithm as summarized below.

10

In the extrapolation problem, $N(\geq 10)$ linear equations from Eqn (14) are used to determine ten coefficients A_α, $\alpha = 1, ..., 10$. Symbolically, it can be written as

$$
\begin{pmatrix}
a_{1,1} & a_{1,2} & \cdots & a_{1,10} \\
a_{2,1} & a_{2,2} & \cdots & a_{2,10} \\
\vdots & \vdots & & \vdots \\
\vdots & \vdots & & \vdots \\
a_{N,1} & a_{N,2} & \cdots & a_{N,10}
\end{pmatrix}
\bullet
\begin{pmatrix}
A_1 \\
A_2 \\
\vdots \\
A_{10}
\end{pmatrix}
=
\begin{pmatrix}
f_1 \\
f_2 \\
\vdots \\
\vdots \\
f_N
\end{pmatrix},
\tag{15}
$$

where $a_{i,1}=1$, $a_{i,2}=(x-x_0)_i$, $a_{i,3}=(y-y_0)_i$, $a_{i,4}=(z-z_0)_i$, $a_{i,5}=(x-x_0)_i^2$,

$a_{i,6}=(y-y_0)_i^2$, $a_{i,7}=(z-z_0)_i^2$, $a_{i,8}=(x-x_0)_i(y-y_0)_i$, $a_{i,9}=(y-y_0)_i(z-z_0)_i$, $a_{i,10}=(x-x_0)_i(z-z_0)_i$,

$f_i = f_i(x,y,z)$.

Eqn (15) is rewritten symbolically below as

$$
X \cdot \beta = Y,
\tag{16}
$$

where X is the matrix of $a_{i,j}$, β is the matrix of A_i and Y is the matrix of f_i. To solve this over-determined linear system (i.e. the number of equations is larger than the number of unknowns.), a linear regression problem needs to be completed via the standard least square minimization protocol [83]. One way is replacing X by its SVD in carrying out the regression of Y on X, as follows. This procedure is also called principal components regression [83].

$$
X \bullet \beta = U
\begin{pmatrix}
\Sigma_{1,1} & 0 & \cdots & 0 \\
0 & \Sigma_{2,2} & \cdots & 0 \\
\vdots & \vdots & \ddots & \vdots \\
0 & 0 & \cdots & \Sigma_{10,10} \\
\vdots & \vdots & & \vdots \\
0 & 0 & \cdots & 0
\end{pmatrix}
V^* \bullet \beta = Y,
\tag{17}
$$

11

where U is a $N \times N$ unitary matrix, V^* is a 10×10 unitary matrix and $\Sigma_{i,i} (i = 1,\ldots,10)$ are the 10

singular values of matrix X. Next β can be calculated directly by multiplying $(X^T X)^{-1} X^T$

to both sides of Eqn (17). Because U, V^* and Σ are known, the solution β is obtained as

$$\beta = \begin{pmatrix} A_1 \\ A_2 \\ \vdots \\ A_{10} \end{pmatrix} = V \begin{pmatrix} \dfrac{1}{\Sigma_{1,1}} & 0 & \cdots & 0 & \cdots & 0 \\ 0 & \dfrac{1}{\Sigma_{2,2}} & \cdots & 0 & \cdots & 0 \\ \vdots & \vdots & \ddots & \vdots & & \vdots \\ 0 & 0 & \cdots & \dfrac{1}{\Sigma_{10,10}} & \cdots & 0 \end{pmatrix} U^* \begin{pmatrix} f_1 \\ f_2 \\ \vdots \\ \vdots \\ f_N \end{pmatrix}. \tag{18}$$

Once the linear system is solved, the potential and gradient of potential (field) at position

(x_0, y_0, z_0) are obtained by the following relation:

$$\begin{aligned}
\phi(x_0, y_0, z_0) &\approx f(x_0, y_0, z_0) = A_1 \\
\phi_x(x_0, y_0, z_0) &\approx f_x(x_0, y_0, z_0) = A_2 \\
\phi_y(x_0, y_0, z_0) &\approx f_y(x_0, y_0, z_0) = A_3 \\
\phi_z(x_0, y_0, z_0) &\approx f_z(x_0, y_0, z_0) = A_4.
\end{aligned} \tag{19}$$

2.6 Linear system solvers

The coefficient matrices produced by the IIM are asymmetric and positive-indefinite. Therefore

the conjugate gradient method or other closely related methods are not suitable for solving these

linear systems. In this study, three general methods, Generalized Minimal RESidual method

(GMRES), BiConjugate Gradient method (BiCG), and algebraic multigrid (AMG) are

investigated to solve these asymmetry linear systems.

Similar to the conjugate gradient method (CG), GMRES constructs a sequence of orthogonal

vectors and minimize the residue along these vectors in sequence. However, for symmetric matrices, only one previous vector is necessary in the construction of the new orthogonal vector. To handle asymmetric matrices, it is necessary to remember all previous vectors and use the Arnoldi iteration to construct the new vector orthogonal to all the previous vectors. GMRES can be summarized as the following pseudo code:

1. Let $l = 0$. Compute residue $r_0 = b - Ax_0$ and set $v_1 = r_0 / \|r_0\|$.
2. Let $l = l + 1$.
3. Use the Arnoldi iteration to construct vector v_{l+1} that is orthogonal to v_k, $k = 0, ..., l$.
4. Minimize the residue along the new vector v_{l+1} and update x_l.
5. Calculate the norm of residues $\|r_l\|$. If $\|r_l\| / \|b\|$ is less than a predefined convergence threshold δ, output x_l as the solution. Otherwise go to step 2.

BiCG is a generalization of conjugate gradient method (CG) for asymmetric and positive-indefinite systems. It constructs two sequences of vectors r_l and $\tilde{r}_l$ which are biorthogonal, that is $r_i^T \tilde{r}_j = \tilde{r}_i^T r_j = 0, i \neq j$. However it constructs the new direction of minimization without the knowledge of previous vectors. Therefore it uses less memory. Apparently, when the matrix A is symmetric, BiCG goes back to CG. However, the method requires two matrix-vector productions at each step. BiCG can be summarized as the following pseudo code:

1. Let $l = 0$. Compute residue $r_0 = b - Ax_0$ and set $\tilde{r}_0 = r_0$, $p_0 = r_0$.
2. Set $l = l + 1$.

3. Calculate $\rho_{l-1} = \tilde{r}_0^T r_0$.

4. If $l = 1$

> set $p_l = r_{l-1}, \ \tilde{p}_l = \tilde{r}_{l-1}$

> Else

> set $\beta_{l-1} = \rho_{l-1} / \rho_{l-2}, \ p_l = r_{l-1} + \beta_{l-1} p_{l-1}, \ \tilde{p}_l = \tilde{r}_{l-1} + \beta_{l-1} \tilde{p}_{l-1}$

5. Calculate $q_l = A p_l, \tilde{q}_l = A^T \tilde{p}_l, \alpha_l = \rho_{l-1} / \tilde{p}_l^T q_l, x_l = x_{l-1} + \alpha_l p_l, r_l = r_{l-1} - \alpha_l q_l, \tilde{r}_l = \tilde{r}_{l-1} - \alpha_l \tilde{q}_l$

6. Calculate the norm of residue $\|r_l\|$. If $\|r_l\| / \|b\|$ is less than a predefined convergence threshold δ, output x_l as the solution. Otherwise go to step 2.

Algebraic multigrid (AMG) was also explored, which is a general multigrid method that does not require any specific structure in the linear system. Further, it does not utilize the geometric information in its operators as in typical multigrid methods. Its generality is important because the regular pattern in the linear system from IIM is lost. According to the original linear system, AMG automatically constructs a series of gradually smaller liner systems, whether the coefficients are continuous or discontinuous. The grids at the finer level C^h are split into two subsets: one set (C^H) includes the grids kept at the coarser level, and the other set (F^H) includes the rest. Then the interpolation operator can be defined as

$$\phi_i^h = \begin{cases} \phi_i^H, & \text{if } i \in C^H \\ \sum_{k \in C^H} w_{ik}^h \phi_k^H, & \text{if } i \in F^H \end{cases}. \tag{20}$$

The restriction operator is the reverse of interpolation operator, and the relaxation operator uses Gauss-Seidel. More grids in subset C^H likely make the interpolation at grids in subset F^H more accurate. On the other hand more grids in C^H consume more computational resource. Therefore a

good grid-splitting algorithm has to balance the interpolation accuracy and computational cost. The detail of the grid-splitting algorithm is reviewed in Ref [84]. In this study, we investigated the performance of a publically available AMG method, AMG1R5, as implemented by Ruge, Stüben and Hempel [85].

CHAPTER 3: Test cases and other computational details

All computational procedures were implemented in the Amber12/PBSA program [9, 11, 13, 14, 78]. The molecular surface was defined using a revised strategy that combines the concept of modified van der Waals surface with an optimized density function [55, 86]. In this strategy, the density function was utilized to smooth the modified van der Waals surface to remove any crevices. The dielectric constant inside ε^- was 1.0, and the dielectric constant outside ε^+ was set at 80.0. All molecules were assigned the charges of Cornell *et al.* [87] and the modified Bondi radii, except that the smallest hydrogen radii were reset to 1.0 Å, i.e. as in the original Bondi radius definition. The probe radius was 1.4 Å. The finite-difference convergence criterion was set to be 10^{-5}. And the Poisson's equation was solved with the charge singularity removed [82].

In the following, the consistency between the new IIM and the classical WHA methods were first investigated to validate the implementation of the new method. The full test cases consisted of 579 biomolecular structures including proteins, nucleic acids and short peptides in the Amber benchmark suite [88]. The atom numbers of these biomolecules range from 247 to 8,254 and their geometries are exceedingly different. These test cases chose 1/2 Å as grid spacing. Then four typical small molecular complexes, adenine-thymine (AT), guanine-cytosine (GC), arginine-aspartic acid (RD) and lysine-aspartic acid (KD) were chosen to analyze the convergence of reaction grid potentials, energies and atomic forces. Molecular surface potentials and fields were also investigated. The grid spacings were chosen as 1/2, 3/8, 1/4, 3/16, 1/8, and

1/16 Å in the AT, GC, RD and KD analyses. Condition numbers of the IIM matrices were also analyzed in the small test systems AT, GC, RD and KD using 1Å as grid spacing due to the large size of the full coefficient matrices. Eight representative proteins were selected to compare the performances of GMRES, BiCG, and AMG linear system solvers. Here, the atom numbers of the selected proteins varied from 1,619 to 4,211. The detail sizes of the selected proteins are showed in Table 1. The total numbers of grid points of these proteins varied from $\sim 2\times10^6$ to 10^7. The tested convergence criteria ranged from 10^{-1} to 10^{-9}.

Table 1.   Eight selected proteins, their No. of atoms (N_{atom}), and No. of x direction grid points times No. of y direction grid points times No. of z direction grid points (N_{grid}).

PROTEIN	N_{atom}	N_{grid}
1a23	2955	175x159x143
1bci	1969	159x111x111
1bxd	2439	191x207x175
1d8v	4211	175x191x175
1fyb	1619	127x175x207
1inz	2413	207x271x191
1qto	1817	143x143x143
2pcf	3884	239x223x159

CHAPTER 4. Results and Discussion

In the following, the IIM implementation was first validated by comparing the numerical reaction field energies of a large set of diversified biomolecules computed by both the IIM and the well-established WHA method. Next the influences of enforcing interface conditions upon the precision of reaction field grid potentials, energies, forces, interface potentials and interface fields were analyzed on a few selected small biomolecular complexes. Finally the performance of different linear system solvers was discussed, which is important for the applications of the IIM in typical biomolecular systems.

4.1 Overall consistency of IIM and WHA on tested biomolecules

As discussed in the Methods section, both the IIM and the WHA method intend to enforce the dielectric boundary conditions, though the WHA method only intends to achieve this approximately. Both methods utilize the same numerically represented surface and the same set of irregular grid points, i.e. grid points with heterogeneous dielectric grid edges. The treatments of the irregular grid points are clearly different between the two methods, as described in detail in the Methods section.

To confirm the implementation of the IIM, reaction field energies of 579 biomolecules were calculated by the IIM and the WHA. The correlation between the numerical energies was shown in Figure 1. Clearly, a very high correlation can be found between the two different algorithms. Detailed analysis shows that the Pearson correlation coefficient is 1.0000 between the two sets of

data, the linear regression slope is 1.0014 (with a fixed offset of zero), and the RMS relative

deviation is 0.0026 between the two sets of data. These data show a very high overall
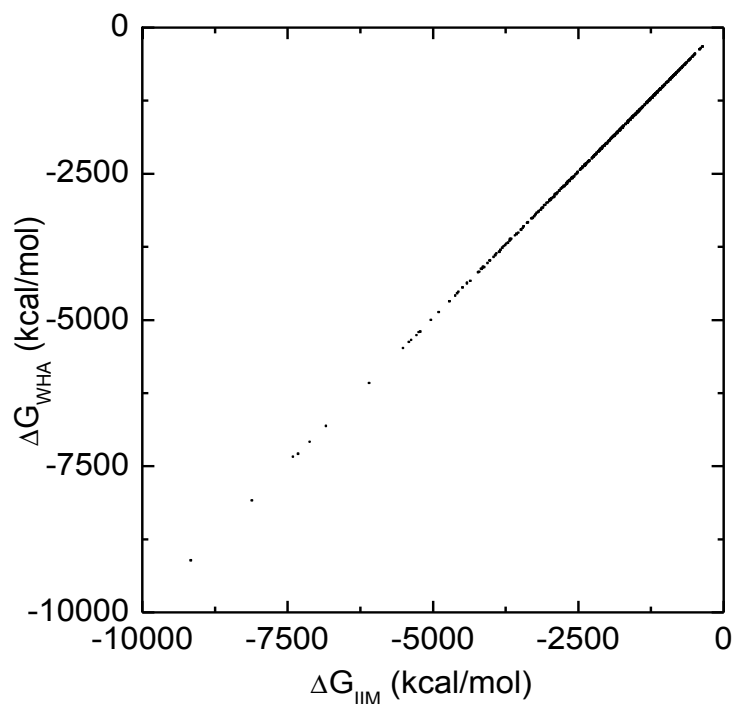
consistency between the two methods.

Figure 1. Correlation of reaction field energies (ΔG) by IIM and WHA at 1/2 Å grid spacing for the Amber training set of 579 biomolecules. The Pearson correlation coefficient is 1.0000 and the linear regression slope is 1.0014 (with fixed offset of zero).

4.2 Convergence of reaction field grid potentials, energies and forces

After validating overall consistency of WHA and IIM, four small molecular complexes (AT, GC,

RD, and KD as described in Methods) were chosen to analyze the convergence of reaction field

grid potentials, atomic reaction field energies, and atomic reaction field forces because these

small systems allow us to use a very fine grid spacing (1/16 Å) for high precision numerical

calculations. Here the numerical results at the 1/16 Å grid were chosen as benchmark due to the lack of analytical solutions for these realistic molecules. Indeed, only very simple models such as monopolar or dipolar spheres allow analytical solution [76].

In this study, the accuracy of the grid potentials and fields nearby each atom was studied using a more detailed calculation instead of the lump-sum total energy that tends to hide local numerical error due to cancellation. Figure 2 shows that the mean absolute errors of the grid potentials at the eight grid points nearby each atom follow similar overall convergence trends, decreasing by a factor of around twenty as the grid spacings reduce from 1/2 to 1/8 Å (with the solutions at 1/16 Å as benchmark). These grid points are the eight nearest grid points in the 1/2 Å FDPB grid whose potentials were computed with different grid spacings, 1/2 Å, 1/4 Å, 1/8 Å and 1/16 Å, respectively, so their potentials can be looked up without any interpolation. Next, the eight nearest grid points of each atom at 1/2 Å, 1/4 Å, 1/8 Å and 1/16 Å FDPB grid were chosen to interpolate the energies and forces with the trilinear mapping method [77]. Figure 3 shows the mean absolute errors of atomic reaction field energies, and Figure 4 presents the mean absolute errors of the atomic reaction field forces. For Figure 3, it is clear that the convergence trends of atomic reaction field energies follow an overall consistent trend between WHA and IIM. The mean absolute errors go down approximately by a factor of twenty when the grid spacings reduce from 1/2 Å to 1/8 Å. For Figure 4, the convergences of atomic reaction field forces are similar to those of energies and potentials, decreasing from ~ 0.04 to ~ 0.002 kcal/mol-Å as the grid spacings reduce from 1/2 to 1/8 Å. The convergence curves in Figure 2, 3 and 4 are not very

smooth because these small molecular systems only have 20-40 atoms each, so the numbers of

sample sizes are not large enough to cancel the fluctuation. In summary, overall similar

convergence behaviors by the two methods are observed in the reaction field grid potentials,

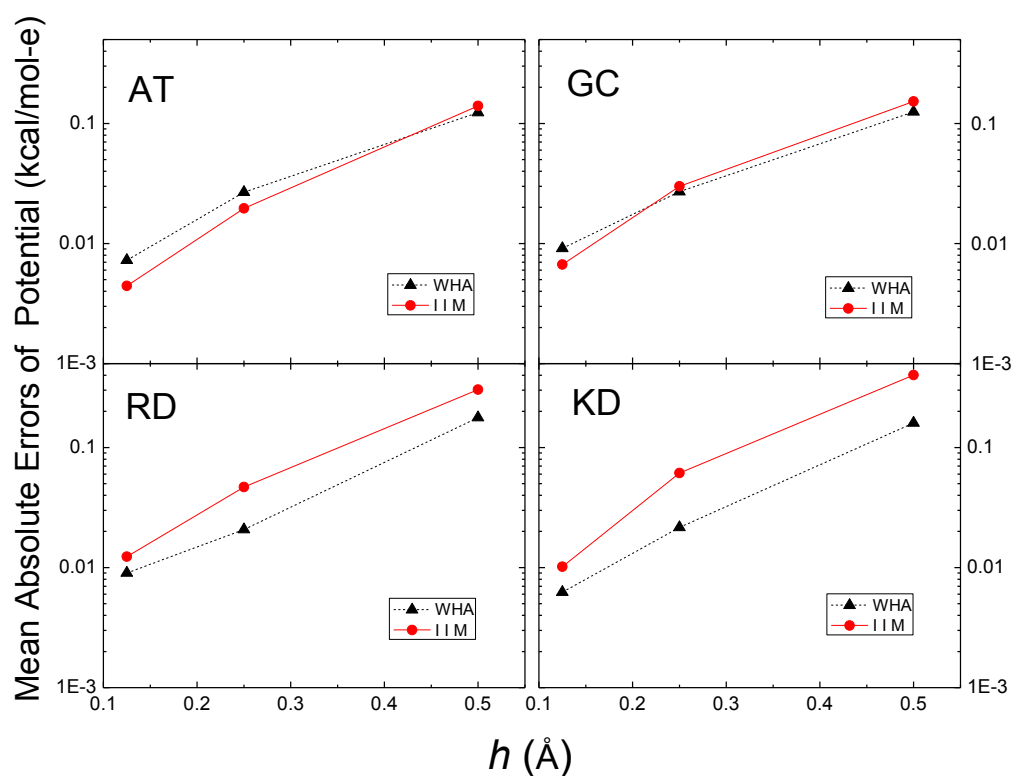atomic reaction field energies and atomic reaction field forces in four tested small complexes.

Figure 2. Mean absolute errors of reaction field potentials at the 8 nearest finite-difference grid points of each atom (kcal/mol-e) versus grid spacing h (Å) with respect to those calculated at the fine grid spacing of 1/16Å for AT, GC, RD and KD dimers, respectively.
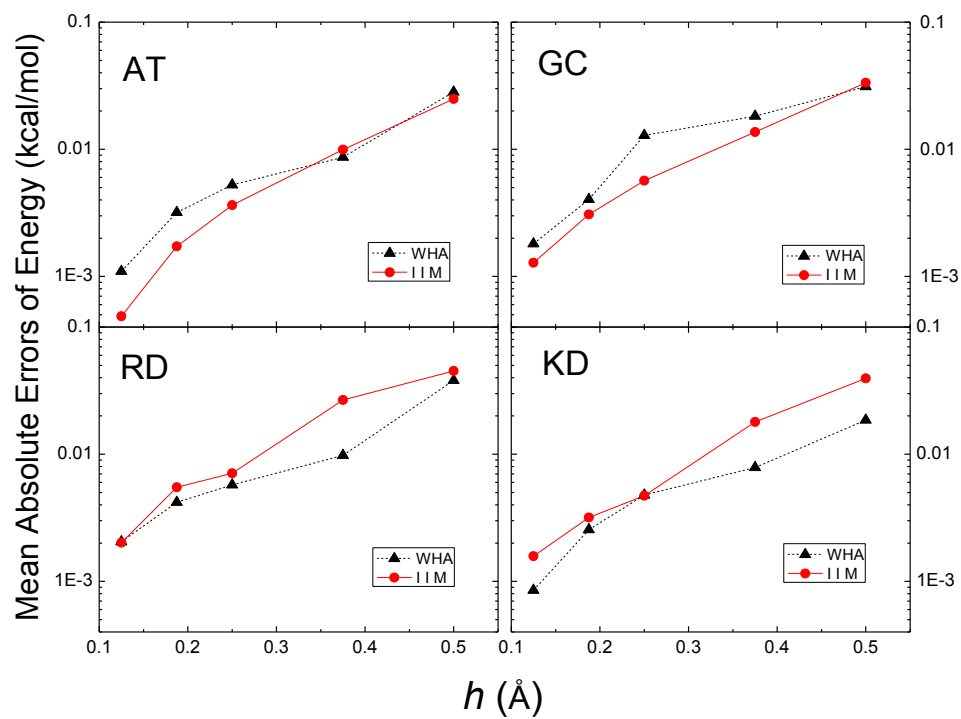
Figure 3. Mean absolute errors of reaction field energies at each atom (kcal/mol) versus grid spacing *h* (Å) with respect to those calculated at the fine grid spacing of 1/16Å for AT, GC, RD and KD dimers, respectively.

Figure 4. Mean absolute errors of reaction field forces at each atom (kcal/mol-Å) versus grid spacing h (Å) with respect to those calculated at the fine grid spacing of 1/16Å for AT, GC, RD and KD dimers, respectively.
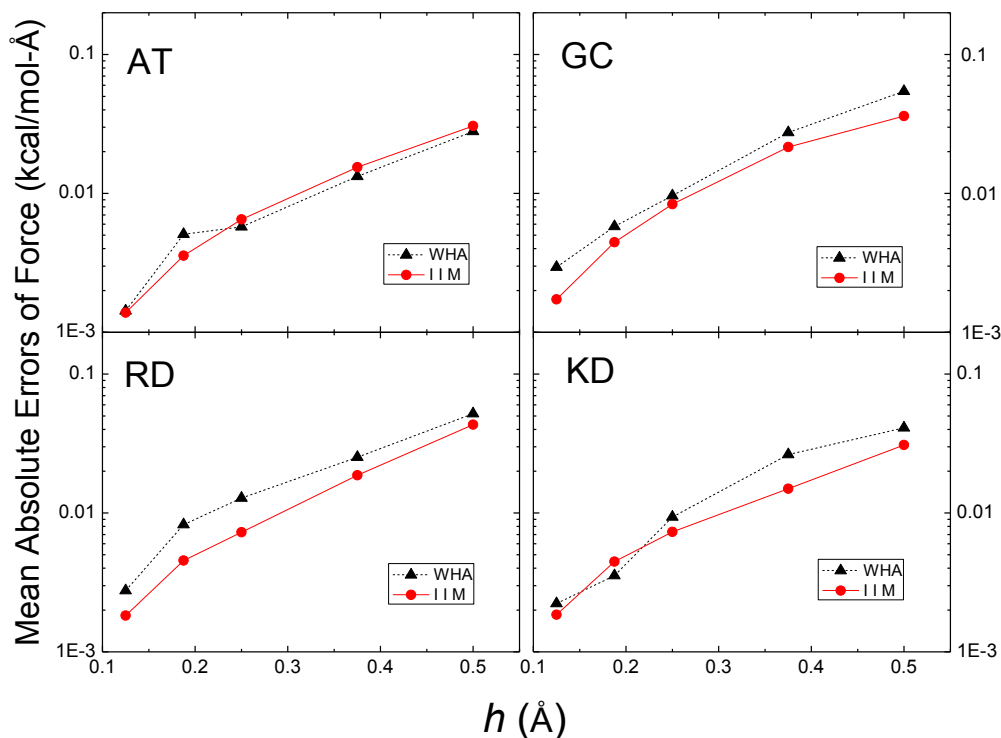
4.3 Convergence of molecular surface potential and field

The IIM intends to offer more accurate numerical solution by enforcing interface jump conditions. Thus there is a good reason to expect IIM to behave more robustly on and nearby the molecular surface. Here AT, GC, RD and KD were again utilized to analyze the quality of numerical surface potential and field by IIM and WHA. As shown in Figure 5, mean absolute errors of inside irregular grid potentials decrease with reducing grid spacing from 1/2 Å to 1/8 Å for both methods: for IIM the errors change from ~0.2 to ~0.01 kcal/mol-e and for WHA the errors change from ~0.6 to ~0.03 kcal/mol-e. The trend lines indicate a significantly consistent

23

smaller errors in the IIM as the inside grid points approach the molecular surface. Comparing with the above analyses on atomic reaction field potentials and atomic reaction field energies, the data show that the benefit of enforcing interface conditions mainly dominates on and nearby the molecular surface, and the benefit is reduced at locations well within the molecular interior.

Extrapolated potential and field on the molecular surface were next analyzed in detail, which are important for dielectric stress and pressure calculation. The extrapolation method is one-side second-order least square fitting method described in the Method section. Figure 6 shows the convergence of the extrapolated interface potentials, giving that the mean absolute errors of IIM are smaller than those of WHA, though the gap between the two convergence trend lines is smaller than that in Figure 5 for the irregular grid points. Here the errors in IIM change from ~0.4 to ~0.02 kcal/mol-e while the errors in WHA is nearly twice as much as those in IIM, from ~0.7 to ~0.04 kcal/mol-e. On the other hand, Figure 7 shows that errors with the almost same order of magnitude were observed in the surface field for both IIM and WHA, reducing from ~2 to ~0.5 kcal/mol-e-Å. There are two possible strategies to improve the extrapolated field on the molecular surface. The first is to apply higher order fitting. Since field is the derivative of potential, the performance of second-order fitting of field should be similar with first-order fitting of potential. Thus, we can expect the third-order fitting of field performs similarly as second-order fitting of potential. The second strategy is to utilize grid points on both sides of the surface during interpolation and to consider the jump conditions across the molecular surface. We will explore these more elaborative methods in a future study.
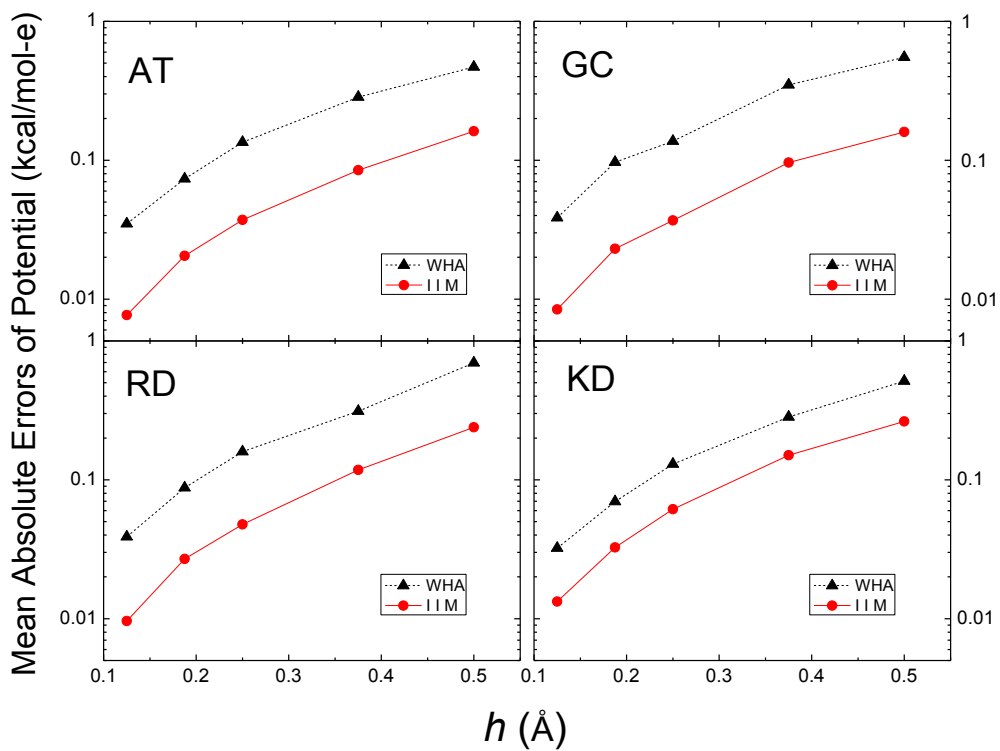
Figure 5. Mean absolute errors of reaction field potentials at the irregular grid points (inside, kcal/mol-e) versus grid spacing h (Å) with respect to those calculated at the fine grid spacing of 1/16Å for AT, GC, RD and KD dimers, respectively.
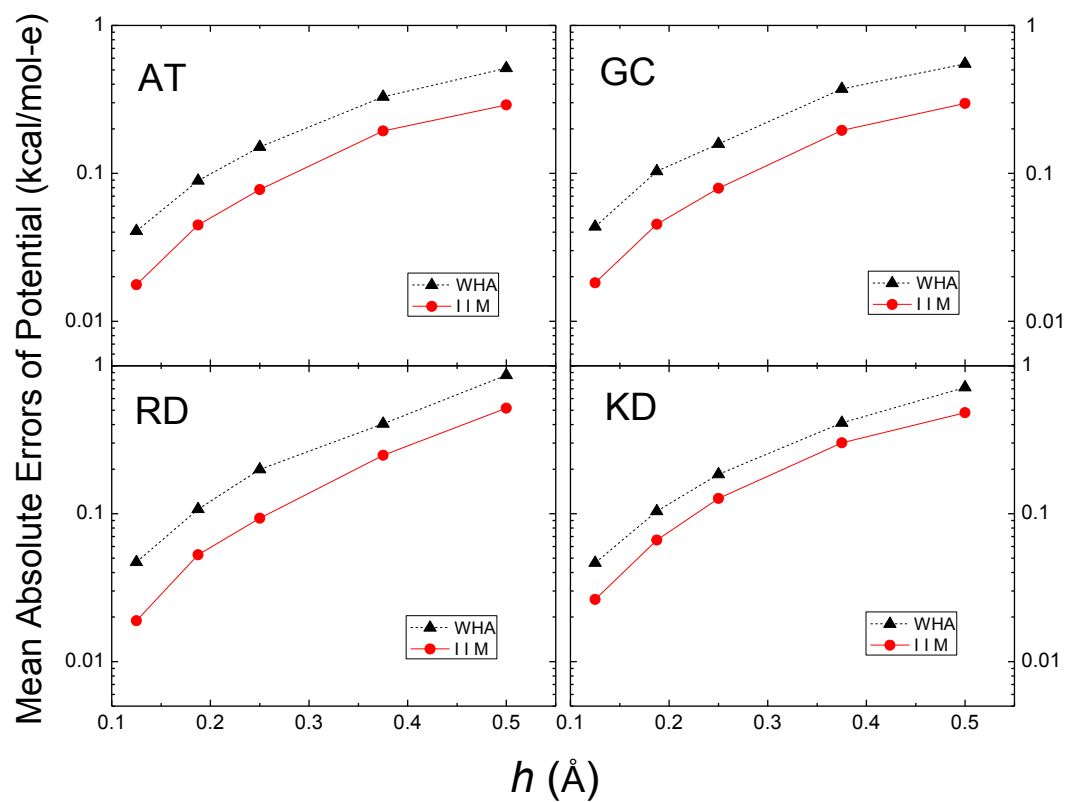
Figure 6. Mean absolute errors of potentials on the molecular surface (inside, kcal/mol-e) versus grid spacing h (Å) with respect to those calculated at the fine grid spacing of 1/16Å for AT, GC, RD and KD dimers, respectively. A second-order least square fitting method was used in all tests.
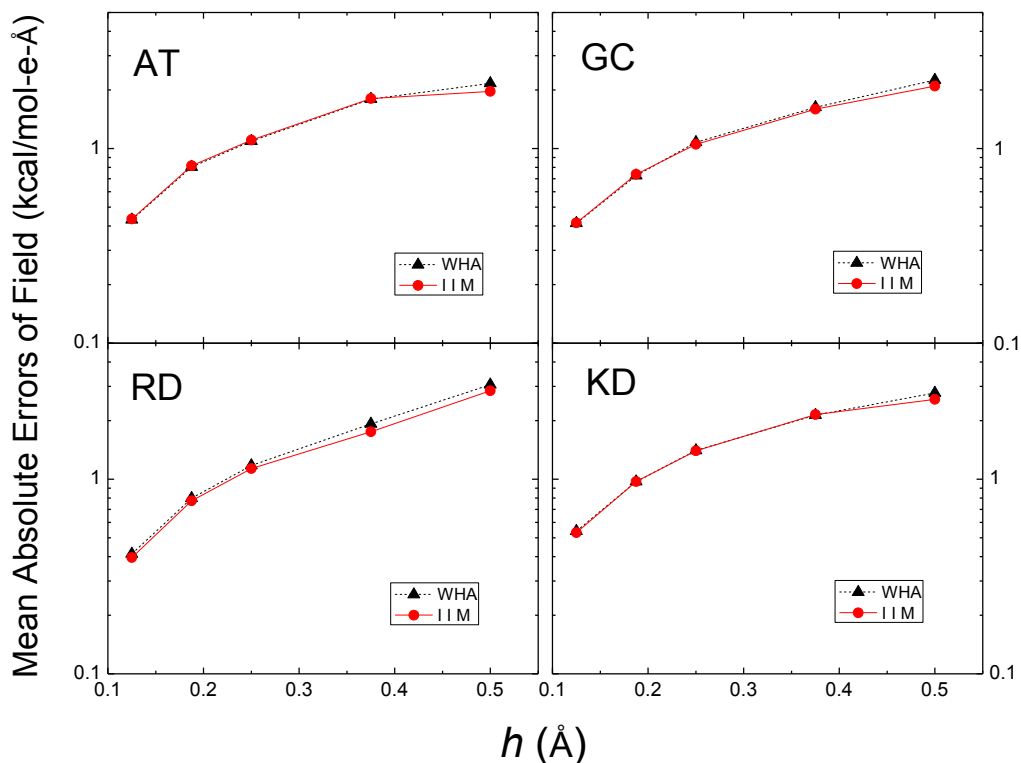
Figure 7. Mean absolute errors of reaction fields on the molecular surface (inside, kcal/mol-e-Å) versus grid spacing h (Å) with respect to those calculated at the fine grid spacing of 1/16Å for AT, GC, RD and KD dimers, respectively. A second-order least square fitting method was used in all tests.

4.4 Condition of IIM matrices and linear system solvers

Before comparing the performance of tested linear system solvers, the condition numbers of IIM matrices were first analyzed as this is a key issue determining the computational efficiency of linear solvers. For a linear algebraic system $A \cdot x = b$, condition number $cond(A)$ is a property of matrix A, showing the rough rate at which solution x changes with respect to the change in b. As reviewed in Methods, the IIM coefficient matrix was constructed to preserve maximum principal. For such matrices the same upper bound holds for the condition number, and can be

27

estimated to be can be estimated as $cond(A) = \dfrac{\max \varepsilon(x,y,z)}{\min \varepsilon(x,y,z)} \dfrac{1}{h^2}$ where $\varepsilon(x,y,z)$ is the

dielectric constant [79]. These have been discussed in detail elsewhere, for example in [89] and

[79]. The IIM was designed to achieve this goal by guaranteeing that the IIM coefficient matrix

is an M-matrix that is diagonally dominant and invertible.

Here we further demonstrate numerically that the IIM coefficient matrices are well

conditioned with the four tested small molecular complexes, AT, GC, RD and KD. The grid

spacings were chosen as 1 Å to keep the coefficient matrices within manageable sizes. Their

reciprocal condition numbers are 7.4×10^{-3}, 1.2×10^{-2}, 1.2×10^{-2}, and 3.0×10^{-2}, respectively. These

numerical analyses agree with the upper-bound estimation mentioned above, indicating the tested

matrices are stable enough, i.e. the solutions do not change dramatically when the right hand

sides are bounded as is the chase of atomic charges in typical biomolecular force fields. Based on

these theoretical discussion and numerical tests, it is reasonable to assume that the IIM matrices

are well conditioned on realistic biomolecules. Indeed convergence is observed for all tested

biomolecules.

Given the theoretical and numerical analysis demonstrating that the IIM linear systems are

well conditioned, we tested three linear system solvers for potential biomolecular applications. It

is instructive first to discuss the memory usage of each solver since the huge memory usage is

always the bottleneck in applying numerical PBE methods in biomolecular simulations. As

described in Methods, both the coefficient matrix and the right-hand-side term are needed during

iteration in all three solvers. In our program, the coefficient matrix is stored in the triad format, requiring $3N_{nz}$ real numbers, where N_{nz} is the number of non-zero element in the coefficient matrix. The right-hand-side term needs to use N_{grid} real numbers, where N_{grid} is the number of the FDPB grid points. Our test shows that AMG needs the most memory: it needs to store $46N_{grid}$ real numbers and $49N_{grid}$ integers. This can be a huge overhead, considering the very high dimensionalities that are often encountered in biomolecular applications. In contrast, both BiCG and GMRES use less memory. BiCG needs $\sim N_{nz}+8N_{grid}$ real numbers and $\sim N_{nz}+4N_{grid}$ integers. Because GMRES retains its previous vectors, it needs more real numbers, $\sim N_{nz}+N_{grid}\times(N_{save}+7)$ real numbers in total, where N_{save} is the number of the saved vectors, set to be 10 in this test. In addition, GMRES also needs $\sim N_{nz}+4N_{grid}$ integers.

An additional disadvantage of AMG is its numerical instability: 5 out of the 579 tested molecules were not able to converge. These failures are unlikely to be memory-related because the tests on many larger molecules were successfully converged. In contrast, tests performed by the GMRES and BiCG solvers on the same set of molecules are both 100% successfully completed. It is difficult to trace down the limitation of the AMG method because of the black-box package [85] that was utilized in our development. Apparently development of a brand new AMG routine may resolve the issue, but it is clearly beyond the scope of this study.

Next the timing of the three tested solvers was analyzed. For the 574 tested molecules that AMG was able to complete successfully, their CPU times are also the longest compared with GMRES and BiCG (data not shown). Thus the two more robust solvers, GMRES and BiCG,

were given more attention below in the following comparative analysis. Figure 8 shows the CPU time versus the number of grid points (N_{grid}). All 579 molecules in the Amber test set were used in this analysis. Nonlinear fits of the timing data indicate that the performance of BiCG is slightly better, scaling as $\sim O(N_{grid}^{1.25})$. GMRES scales as $\sim O(N_{grid}^{1.28})$. However, there are significant deviations in the GMRES trend line, indicating a less robust performance among individual tested molecules.

Finally the relation between CPU time and the relative convergence criterion is analyzed and shown in Figure 9. The eight proteins listed in Table 1 were used as examples. Overall, similar performances between GMRES and BiCG were observed, consistent with the above analysis on the relation between CPU time and the linear system sizes. However, the performance of GMRES fluctuates greatly even for the eight relatively smaller proteins. For example, GMRES is about one to two times slower than BiCG for 1a23 and 1inz to reach the relative convergence criterion of 10^{-9}.
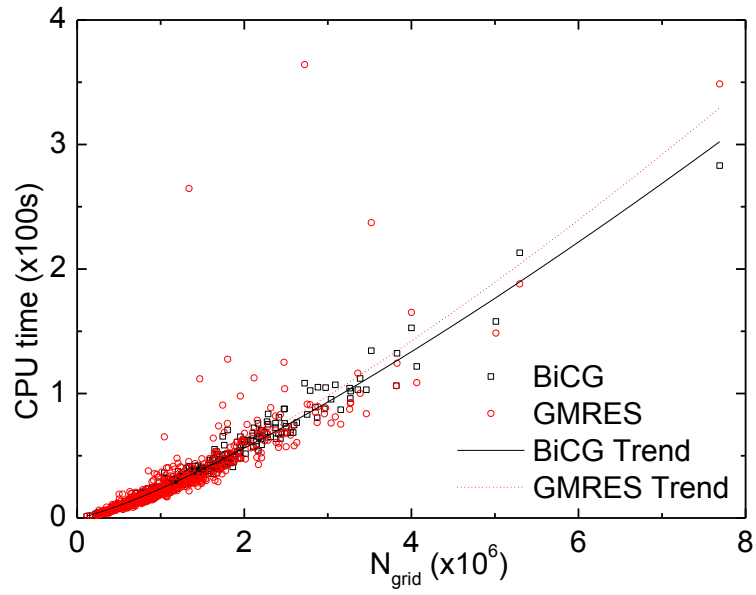
Figure 8. CPU time versus the number of grids (N_{grid}) for GMRES and BiCG, respectively. Convergence criterion (relative) is set to be 10^{-6}.
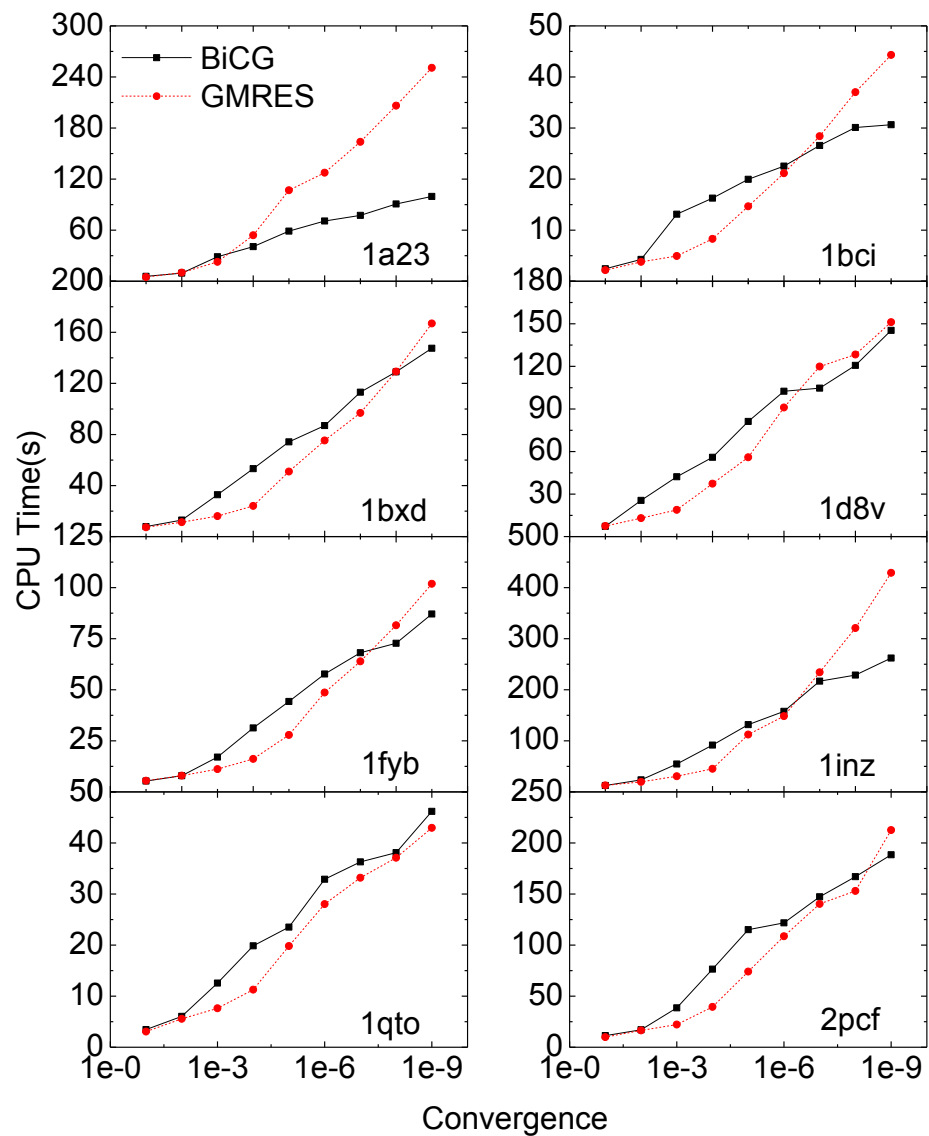
Figure 9. CPU time versus convergence criterion for GMRES and BiCG, respectively, for the eight proteins listed in Table I.

CHAPTER 5. Conclusion and Future Directions

We have explored a higher-accuracy numerical scheme, the immersed interface method, to solve the Poisson-Boltzmann equation for biomolecular applications. The implementation of the new method was first validated for applications on realistic biomolecules using a diversified set of biomolecules by comparing reaction field energies computed by the new method and the well-established classical weighted harmonic averaging method. Overall a very high correlation was found between the two set of energies, given the clearly different treatments of the interface grid points as described in detail in the Methods section.

With the overall consistency of the two methods, we went ahead to analyze the convergence of reaction field grid potentials, atomic reaction field energies, and atomic reaction field forces using several tested small molecular complexes. Overall a similar convergence behavior was observed with the mean absolute errors that decrease by a factor of around twenty from 1/2 Å to 1/8 Å grid spacings for both methods. We further analyzed the quality of numerical surface potential and field by the two methods. The convergence behavior of boundary grid potentials is similar for both methods, but apparently smaller errors were observed for the new method, which were around 1/3 of those for the classical method. Surface potentials and fields, extrapolated by the one-side second-order least square fitting method, converge similarly as boundary grid potentials for both methods. Nevertheless, larger errors were observed for the surface potentials compared with the errors of boundary grid potentials, though the errors of new method is still around half of the classical method, showing the advantage in surface potentials analyses.

33

However, the errors in the surface field by the new method are virtually identical to those by the classical method.

Apparently we need to further improve the extrapolation scheme on the molecular surface to bring out the higher accuracy observed on the grid potentials by utilizing the higher ordered new method. In the current study, extrapolated surface field, as one of key physical quantities, has not benefitted from using the higher accuracy scheme, limiting the realistic application prospects of the new method. We are actively exploring to improve the accuracy of the surface field from developing higher-order fitting procedures and applying higher weights to grid potentials closer to the surface point of interest. We are also developing two-side least square fitting methods to utilize the dielectric boundary condition to reduce fitting errors.

References

[1] I. Klapper, R. Hagstrom, R. Fine, K. Sharp, and B. Honig, Proteins Structure Function and Genetics **1** (1986).

[2] M. E. Davis and J. A. McCammon, J. Comput. Chem. **10** (1989).

[3] A. Nicholls and B. Honig, J. Comput. Chem. **12** (1991).

[4] B. A. Luty, M. E. Davis, and J. A. McCammon, J. Comput. Chem. **13** (1992).

[5] M. Holst and F. Saied, J. Comput. Chem. **14** (1993).

[6] K. E. Forsten, R. E. Kozack, D. A. Lauffenburger, and S. Subramaniam, J. Phys. Chem. **98** (1994).

[7] W. Im, D. Beglov, and B. Roux, Comput. Phys. Commun. **111** (1998).

[8] W. Rocchia, E. Alexov, and B. Honig, J. Phys. Chem. B **105** (2001).

[9] R. Luo, L. David, and M. K. Gilson, J Comput. Chem. **23** (2002).

[10] D. Bashford, Lecture Notes in Computer Science **1343** (1997).

[11] Q. Lu and R. Luo, J Chem. Phys. **119** (2003).

[12] N. V. Prabhu, P. J. Zhu, and K. A. Sharp, J Comput. Chem. **25** (2004).

[13]J. Wang and R. Luo, J Comput. Chem. **31** (2010).

[14]Q. Cai, M. J. Hsieh, J. Wang, and R. Luo, J Chem. Theory Comput. **6** (2010).

[15]C. M. Cortis and R. A. Friesner, J. Comput. Chem. **18** (1997).

[16]N. Baker, M. Holst, and F. Wang, J. Comput. Chem. **21** (2000).

[17]M. Holst, N. Baker, and F. Wang, J. Comput. Chem. **21** (2000).

[18]A. I. Shestakov, J. L. Milovich, and A. Noy, Journal of Colloid and Interface Science **247** (2002).

[19]L. Chen, M. J. Holst, and J. C. Xu, Siam Journal on Numerical Analysis **45** (2007).

[20]D. Xie and S. Zhou, BIT Numerical Mathematics **47** (2007).

[21]M. Friedrichs, R. H. Zhou, S. R. Edinger, and R. A. Friesner, J Phys. Chem. B **103** (1999).

[22]S. D. Bond, J. H. Chaudhry, E. C. Cyr, and L. N. Olson, J Comput. Chem. **31** (2010).

[23]B. Lu, M. J. Holst, J. A. McCammon, and Y. C. Zhou, J Comput Phys **229** (2010).

[24]B. Z. Lu and Y. C. Zhou, Biophys J **100** (2011).

[25]S. Miertus, E. Scrocco, and J. Tomasi, Chemical Physics **55** (1981).

[26]H. Hoshi, M. Sakurai, Y. Inoue, and R. Chujo, Journal of Chemical Physics **87** (1987).

[27] R. J. Zauhar and R. S. Morgan, J. Comput. Chem. **9** (1988).

[28] A. A. Rashin, J. Phys. Chem. **94** (1990).

[29] B. J. Yoon and A. M. Lenhoff, J. Comput. Chem. **11** (1990).

[30] A. H. Juffer, E. F. F. Botta, B. A. M. Vankeulen, A. Vanderploeg, and H. J. C. Berendsen, J. Comput. Phys. **97** (1991).

[31] H. X. Zhou, Biophys. J. **65** (1993).

[32] R. Bharadwaj, A. Windemuth, S. Sridharan, B. Honig, and A. Nicholls, J. Comput. Chem. **16** (1995).

[33] E. O. Purisima and S. H. Nilar, J. Comput. Chem. **16** (1995).

[34] J. Liang and S. Subramaniam, Biophys. J. **73** (1997).

[35] Y. N. Vorobjev and H. A. Scheraga, J. Comput. Chem. **18** (1997).

[36] M. Totrov and R. Abagyan, Biopolymers **60** (2001).

[37] A. H. Boschitsch, M. O. Fenley, and H. X. Zhou, J. Phys. Chem. B **106** (2002).

[38] B. Z. Lu, X. L. Cheng, J. F. Huang, and J. A. McCammon, Proceedings of the National Academy of Sciences of the United States of America **103** (2006).

[39] B. Z. Lu, X. L. Cheng, T. J. Hou, and J. A. McCammon, J Chem. Phys. **123** (2005).

[40] B. Z. Lu, D. Q. Zhang, and J. A. McCammon, J Chem. Phys. **122** (2005).

[41] B. Z. Lu, X. L. Cheng, J. F. Huang, and J. A. McCammon, J Chem. Theory Comput. **5** (2009).

[42] C. Bajaj, S. C. Chen, and A. Rand, Siam J Sci Comput **33** (2011).

[43] M. E. Davis and J. A. Mccammon, J Comput. Chem. **12** (1991).

[44] Y. C. Zhou, S. Zhao, M. Feig, and G. W. Wei, Journal of Computational Physics **213** (2006).

[45] W. H. Geng, S. N. Yu, and G. W. Wei, J Chem. Phys. **127** (2007).

[46] S. N. Yu and G. W. Wei, Journal of Computational Physics **227** (2007).

[47] Y. C. Zhou, M. Feig, and G. W. Wei, Journal of Computational Chemistry **29** (2008).

[48] Q. Zheng, S. Y. Yang, and G. W. Wei, Int J Numer Meth Bio **28** (2012).

[49] J. Dzubiella, J. M. J. Swanson, and J. A. McCammon, J Chem. Phys. **124** (2006).

[50] J. Dzubiella, J. M. J. Swanson, and J. A. McCammon, Phys. Rev. Lett. **96** (2006).

[51] L. T. Cheng, J. Dzubiella, J. A. McCammon, and B. Li, J Chem. Phys. **127** (2007).

[52] Z. Chen, S. Zhao, J. Chun, D. G. Thomas, N. A. Baker, P. W. Bates, and G. W. Wei, J Chem. Phys. **137** (2012).

[53]D. G. Thomas, J. Chun, Z. Chen, G. W. Wei, and N. A. Baker, J Comput. Chem. **34** (2013).

[54]J. Wang, Q. Cai, Y. Xiang, and R. Luo, J Chem. Theory Comput. **8** (2012).

[55]W. M. Botello-Smith, X. P. Liu, Q. Cai, Z. L. Li, H. K. Zhao, and R. Luo, Chem. Phys. Lett. **555** (2013).

[56]M. E. Davis, J. D. Madura, and J. A. Mccammon, Biophys J **57** (1990).

[57]K. Sharp, J. Comput. Chem. **12** (1991).

[58]C. Niedermeier and K. Schulten, Molecular Simulation **8** (1992).

[59]M. K. Gilson, M. E. Davis, B. A. Luty, and J. A. McCammon, J. Phys. Chem. **97** (1993).

[60]M. K. Gilson, J. Comput. Chem. **16** (1995).

[61]A. A. Rashin, J. Phys. Chem. **93** (1989).

[62]Y. N. Vorobjev, J. A. Grant, and H. A. Scheraga, J. Am. Chem. Soc. **114** (1992).

[63]B. J. Yoon and A. M. Lenhoff, J. Phys. Chem. **96** (1992).

[64]R. J. Zauhar and R. S. Morgan, J. Mol. Biol. **186** (1985).

[65]B. A. Luty, M. E. Davis, and J. A. McCammon, Journal of Computational Chemistry **13** (1992).

[66] C. M. Cortis and R. A. Friesner, J. Comput. Chem. **18** (1997).

[67] L. D. Landau, E. M. Lifshitz, and L. P. Pitaevskii.

[68] J. Che, J. Dzubiella, B. Li, and J. A. McCammon, J. Phys. Chem. B **112** (2008).

[69] Q. Cai, X. Ye, J. Wang, and R. Luo, Chem. Phys. Lett. **514** (2011).

[70] B. Li, X. Cheng, and Z. Zhang, Siam Journal on Applied Mathematics **71** (2011).

[71] Q. Cai, X. Ye, and R. Luo, Phys. Chem. Chem. Phys. **14** (2012).

[72] R. J. Zauhar, J. Comput. Chem. **12** (1991).

[73] M. E. Davis and J. A. Mccammon, J Comput. Chem. **11** (1990).

[74] R. E. Bruccoleri, J. Comput. Chem. **14** (1993).

[75] R. J. LeVeque and Z. Li, SIAM J. Numer. Anal. **31** (1994).

[76] J. Wang, Q. Cai, Z. L. Li, H. K. Zhao, and R. Luo, Chem. Phys. Lett. **468** (2009).

[77] D. T. Edmonds, N. K. Rogers, and M. J. E. Sternberg, Molecular Physics **52** (1984).

[78] Q. Cai, X. Ye, J. Wang, and R. Luo, J Chem. Theory Comput. **7** (2011).

[79] Z. L. Li and K. Ito, *The Immersed Interface Method: Numerical Solutions of PDEs Involving Interfaces and Irregular Domains* (SIAM, Society for Industrial and Applied Mathematics, Philadelphia, 2006), Frontiers in Applied Mathematics.

[80] Z. X. Zhou, P. Payne, M. Vasquez, N. Kuhn, and M. Levitt, J Comput. Chem. **17** (1996).

[81] I.-L. Chern, J.-G. Liu, and W.-C. Wang, Methods and Applications of Analysis **10** (2003).

[82] Q. Cai, J. Wang, H. K. Zhao, and R. Luo, J Chem. Phys. **130** (2009).

[83] J. Mandel, Am Stat **36** (1982).

[84] K. Stuben, Journal of Computational and Applied Mathematics **128** (2001).

[85] J. W. Ruge and S. K., in *Multigrid Methods*, edited by S. F. McCormick (SIAM, Philadelphia, 1987), pp. 73.

[86] X. P. Liu, C. H. Wang, J. Wang, Z. L. Li, H. K. Zhao, and R. Luo, Phys. Chem. Chem. Phys. **15** (2013).

[87] W. D. Cornell *et al.*, J. Am. Chem. Soc. **117** (1995).

[88] D. A. Case *et al.*, *Amber 10* (University of California, San Francisco, 2008).

[89] Z. L. Li and K. Ito, Siam J Sci Comput **23** (2001).